How Pulars Provide Some Observational Constraints on Theoretical Models

A. Jessner

(*Max-Planck-Institut für Radioastronomie, Auf dem Hügel 69, D-53121Bonn, Germany*)

Abstract Pulsar observations at Effelsberg have a long history and cover a wide frequency range (800 MHz — 43 GHz). Our equipment enables us to make high quality radio observations in all important aspects of pulsar study.

High precision pulsar timing observations enabled us to find an upper limit to the radius of the companion star close to the theoretical minimum from the influence of spin-orbit coupling on the orbital parameters of PSR J2051–0827. Studies of interstellar scattering for nine pulsars with high dispersion measure show a much flatter dependence of the scattering time with frequency than predicted by simple single screen Gaussian or Kolmogorov ISM models. A determination of rotation measure for 46 pulsars enabled us to conclude, that no large scale reversals of the magnetic field occur within 85 deg $< l <$ 245 deg and the magnetic field follows the local spiral closely between 150 deg $< l <$ 245 deg, but the turbulent structure of the intervening field defies modelling with a single scale height and typical size of the random magnetic field component. Investigating single pulses of PSR B0329+54 simultaneously received in Jodrell Bank and Effelsberg, it became evident, that between the two frequencies, the centre component correlates strongly for circular polarisation, but not for linear polarisation, whereas both outer components exhibit the converse behaviour. The emission process has a wide bandwidth, but the outer (conal) profile components cannot originate at a lower height compared to the central component, if the observed fluctuations are to be a magnetospheric propagation effect. Pulsars also show unexpected behaviour at the very high radio frequencies ($>$ 10GHz) where they are still visible,- if only for the Effelsberg instrument. In a number of cases the received fluxes are higher than expected, suggesting an up-turn in their spectrum. Furthermore, their variability is higher than predicted and it is likely that we observe intrinsic intensity variations at these frequencies. Observations indicate that radioemission is generated within the light-cylinder, but that fact in itself places a tight upper limit on the product of particle density and Lorentz factor. In the case of the crab pulsar, this density is much less than the assumptions of standard pulsar models. Coherent curvature radiation is also shown to be too inefficient to account for radio emission below 10-20 GHz.

1 High Precision Pulsar Timing: Spin-Orbit Coupling in the J2051–0827 System

The eclipsing binary pulsar J2051–0827 was discovered at Parkes (Stappers et. al. 1996). It has a very short orbital period of $P_b > 2.4$ hrs and an almost circular orbit, eclipsing about 10% of the orbital period. The companion is a white dwarf with $0.027 M_{sun} < m_{comp} < 0.055 M_{sun}$. The semi-major axis has a radius of $1.03 R_{sun}$ and the orbital period decreases at a rate of $\dot{P}_b = -15.8(8) \cdot 10^{-12}$ which implies a decay time of about $\sim 25 \cdot 10^6$ years. Observations were made in Effelsberg (0.86, 1.4, 1.7, 2.7 GHz) and Jodrell Bank (0.325, 0.41, 0.61, 1.4 GHz) for over 6.5 yrs yielding 584 TOA's (Doroshenko et al., 2001).

A complete orbit was observed each time, but orbital phases from 0.2 to .35 (near the eclipse) were excluded from the fit. The TOA's were fitted using the TIMAPR package (Dorsohenko & Kopeikin 1995) with average post-fit residuals of $\sigma = 21.2\mu$s. A number of effects, such as the emission of gravitational waves, acceleration of the binary system, mass loss from the system, tidal dissipation and gravitational quadrupole coupling can in principle contribute to the observed orbital decay. We found however, that except for the case of gravitaional quadrupole coupling, the mentioned effects are too small by at least two orders of magnitude if compared to the observed value (Doroshenko et al., 2001). We also measured the second derivative of P_b as $\ddot{P}_b = +2.1(3) \cdot 10^{-20}\mathrm{s}^{-1}$. Its magnitude implies that the presently decreasing orbital period will begin to increase after $-2\dot{P}_b/\ddot{P}_b \sim 33$yrs and the that the system is undergoing quasi-periodic oscillations with a cyclic spin-up and spin-down similar to PSR B1957+20. Like in some normal stellar binaries (Algol, RS CV) the outer layers of the companion of J2051-0807 are thought to spin up and down in cycles providing a variable inertial quadrupole moment and an exchange between orbital angular momentum **L** and spin of the companion **S**. This will result in a precession of both **L** and **S** which can be detected as a variation of the projected semi-major axis a. Our measurements yielded * $\dot{x} = -23(3) \cdot 10^{-14}\mathrm{s} \cdot \mathrm{s}^{-1}$. In this case the semi-major axis a_p will remain constant, but its projection $x = a_p \sin i$ will undergo secular variations resulting in a change of the inclination of $\frac{di}{dt} = \frac{\dot{x}}{x} \tan i$. Depending on the actual inclination $30\,\mathrm{deg} < i < 89\,\mathrm{deg}$ we get a range of change for i as $0.007\,\mathrm{deg\,yr}^{-1} < di/dt < 0.67\,\mathrm{deg\,yr}^{-1}$. Again, an investigation of other possible causes of the inferred $\dot{x}$ showed them to be too small by four to five orders of magnitude. For spin-orbit coupling, the secular change of i depends on the fifth power of the radius R_c of the companion:

$$\frac{di}{dt} = \frac{\Omega_b}{2} \frac{k_{\mathrm{apsid}} R_c^2}{a_p(1-e^2)} \frac{\Omega_c^2 R_c^3}{\Gamma m_c}\,, \tag{1}$$

here k_{apsid} is the apsidal motion constant and for synchronous rotation of the companion the orbital Ω_b and companion spin Ω_c frequencies are the same. One can thus find an upper limit for the radius of companion of $R_c < 0.06 R_{\mathrm{sun}}$ and a most probable value of $R_c \leq 0.03 R_c$ for $i = 40\,\mathrm{deg}$. The upper limit is still only half the minimum size of the Roche lobe $R_L = 0.13 R_{\mathrm{sun}}$ for a $0.027 M_{\mathrm{sun}}$ companion, but the most probable value is alarmingly close to the minimum size of the smallest $0.027 M_{\mathrm{sun}}$ star, a pure He white dwarf. In fact, B.P. Gong (these proceedings) has pointed out that the spin-orbit coupling of the neutron star itself will also contribute to $\frac{di}{dt}$ which would make that estimate even tighter.

2 Scatter Broadening: An Example of a Multifrequency Profile Study

On its way from the source the pulsar signal is scattered by inhomogeneities in the interstellar medium, propagates on multiple paths and thus aquires random phases. This results in an exponential tail in the observed pulsar profile $P_{obs}(t)$ which can be described as a convolution of the unscattered profile $P_0(t)$ with an exponential scattering kernel

$$P_{obs} = P_0(t) \otimes e^{\frac{-t}{\tau_{sc}}}\,, \tag{2}$$

where τ_{sc} is the scattering timescale. Profiles of nine highly dispersed pulsars were obtained in Effelsberg (1.4, 2.7 and 4.9 GHz) and in Jodrell Bank (0.6, 0.9 and 1.4 GHz). They were

*distances are given as light travel times

carefully selected for negligible profile evolution (Löhmer et al, 2001). Their outer pulse components have flatter spectra and pulse widths decrease with increasing frequency. These effects are however quite small above 1 GHz. Their decorrelation bandwidth $\Delta\nu \sim 50$Hz at 1 GHz is hard to measure, hence these were the first measurements of the scattering spectral index for high-DM pulsars.

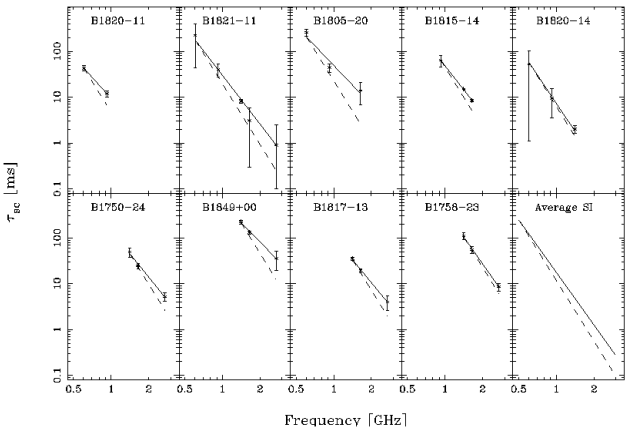

Fig. 1 The graph shows the average scatter broadening time for the nine objects with their 3σ errors and a power-law fit. Dashed lines are examples of the expected dependence from a Kolomogorov spectrum with $\nu^{-4.4}$. The lower rightmost panel shows the observed average dependency of $\tau_{sc} \propto \nu^{-3.4\pm0.13}$.

A fit of several Gaussian components to the high-frequency (4.85 GHz) profile was used as a template for convolution with the exponential scattering kernel. The optimal scattering time was determined for each frequency, by fitting the convolved templates to the observations. In contrast to previous measurements of low DM objects which were compatible with a $\tau_{sc} \propto \nu^{-4.4}$ Kolmogorov spectrum (Cordes et al., 1985; Johnston et al., 1998), highly dispersed pulsars show a much flatter decay of τ_{sc} than even the simple Gaussian model (Lambert & Rickett 1999) with it $\tau_{sc} \propto \nu^{-4}$ dependence. While individual measurements may indeed be affected by the geometry and spectral model represented by the 3σ error bars , their trend isn't and the derived spectral index cannot be an artifact of the template fitting procedure. An attempt was also made to use an alternative scattering kernel $t^{-1/2}e^{\frac{-t}{\tau_{sc}}}$ (Cordes, priv. comm.) but this could not fit the scattering tail as accurately as the simple exponential.

A simple model with a single thin screen cannot describe the observed frequency dependence for high DM pulsars. But multiple screens of smaller transverse extent could in principle flatten the frequency dependence by reducing the amount of scattering at lower frequencies

3 Rotation Measures And The Large Scale Structure of The Galactic Magnetic Field

Pulsars are excellent probes of the ISM and the magnetic field. From a determination of the rotation measure RM and the dispersion measure DM one can calculate the effective magnetic field projected onto the line of sight $B_{||} = 1.23\frac{RM}{DM}\mu$G. For the observations we

used the coherent Effelsberg-Berkeley Pulsar Processor (EBPP) in its bandspread mode, providing 4 x 8 polarisation channels across the receiver band width of 98 MHz. The bandwidth of each of the individual 32 channels depends on the DM of the observed pulsar, but is limited to 0.875 MHz for the polarization mode at around 1.4 GHz. In total, a bandwidth of 28 MHz is avaliable, spread around in four sub-bands of 7 MHz, placed at the very edges of the receiver bandwidth and in two symmetrically placed central regions. All signals are detected and folded in phase with the topocentric pulsar period. Each sub-integration, which typically lasts for 180–300 s, is transferred to a computer for offline processing. The four Stokes parameters are computed for each of the 32 channels and a RM search is made so that their superposition maximises the linear polarisation. Altogether 45 PSR's were observed in that mode, but only 35, unaffected by electron density anomalies like HII regions and SNRs, were selected to estimate the effective magnetic field strength of the Perseus arm within $85\,\mathrm{deg} < l < 245\,\mathrm{deg}$ and $|b| < 10\,\mathrm{deg}$. We consider a model where the regular uniform magnetic field of magnitude B_o traces the spiral arm as depicted by Georgelin & Georgelin (1976) and use a cubic spline fit as adopted by Taylor & Cordes (1993) to construct the spiral arm. For each respective Galactic longitude of the pulsar we obtain the direction of $\vec{B_\mathrm{o}}$, we then project onto the radial vector to obtain B_p as a function of l. The resulting dependence of B_p on l is then used to fit the data points. In addition to the field strength, B_o, we allow for another free parameter to be determined, i.e. θ which describes the possibility that the so called 'magnetic arm' might actually be at an angle with respect to the spiral arm, a circumstance which is also commonly observed in external galaxies (Beck 2000). A positive value of θ would mean that the spiral arm needs to be rotated around the Galactic Centre in the counter clockwise direction by that amount to match the 'magnetic arm' to the regular component of the field. A least-square fit (Mitra et al. 2002) to the data gives B_o as 1.5 ± 1 μG and $\theta = 12° \pm 8°$. The estimate of B_o is consistent with that of Lyne & Smith (1989). But even with the carefully selected sources we find a great variability of $B_{||}$ in our data and evidently a model with a uniform magnetic field along the spiral arm, or even along the line-of- sight is too simple! In fact we should expect random variations of the electron density n_e, as was indicated i.e. by scattering (see above)! Similarly, the fit residuals should reflect the distance D dependence along the "random walk" through the variable field: $\sigma_\mathrm{rm}(D) = 0.81 \times \delta n_e B_r \sqrt{L_r D}\mathrm{rad\,m^{-2}}$. Here $B_r \sim 5\mu$G is the typical amplitude of the random magnetic field component, and $L_r \sim 30pc$ the scale of the the field fluctuations. The density fluctuations and their correlation with $B_{||}$ are unknown, hence their size δn_e was assumed to be of order unity and only B_r remained as a free parameter. However, if B_o and the product $\delta n_e B_r \sqrt{L_r}$ were independent of the distance, we would find the expected square root dependence of $\sigma \propto \sqrt{D}$. From our data, and from previous work by Rand & Kulkarni (1989), we cannot confirm such a simple view of the turbulent structure of the ISM and its magnetic field.

4 Multifrequency Single Pulse Polarisation Study of PSR 0329+54

Simultaneous multifrequency pulsar observations are an obvious way of investigating the radio emission region more closely. First studies were made by Bartel and Sieber (1978) at 0.3 GHz and 2.7 GHz using both Effelsberg and Jodrell Bank in total power mode. The data processing of simultaneous observations is much easier if a common data format is supported by the participating observatories. In 1995, the EPN, the European Pulsar Network was launched to further the cooperation of European pulsar astronomers and one of its successes was the definition of such a common data format (Lorimer, Jessner, Seiradakis et. al. 1998) and a public on-line database (http://www.mpifr-bonn.mpg.de/div/pulsar/data)

of profiles and spectra. The EPN format is now supported by a large number of radio-observatories, amongst them Effelsberg, Jodrell Bank, Bologna, Westerbork, Pushchino, Torun, Ooty and GMRT. The existence of the new standard format has made it easy and nearly a routine matter to participate in simultaneous multifrequency-multitelescope single pulse pulsar observations with our partners in Europe and in India. In the case at hand 1912 single pulses of PSR B0329+54 were recorded simultaneously with a $S/N > 100$ in Effelsberg (2.695 GHz, BW 80 MHz) and Jodrell Bank. Calibrated and aligned EPN data was then rebinned (Karastergiou et al. 2001) to a common time resolution. We find that

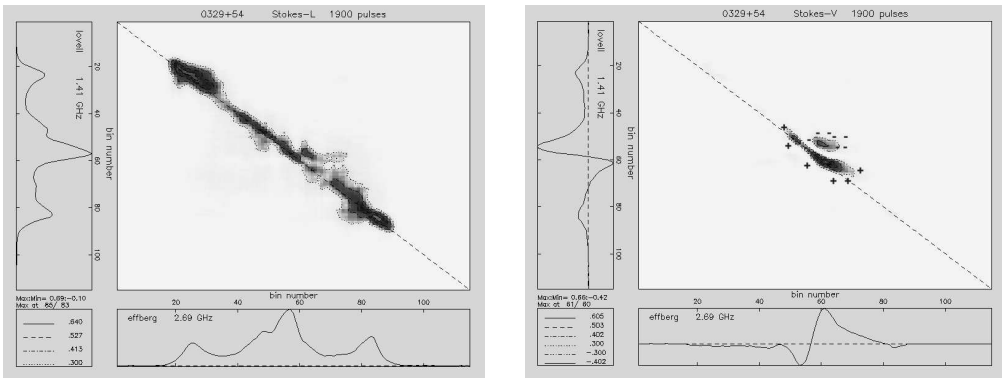

Fig. 2 Cross-correlation contours for linear (left) and circular polarisation (right) of single pulses from PSR B0329+54, received at 1.41 GHz (vertical direction) and 2.69 GHz (horizontal direction). For circular polarisation, the sign of the correlation is marked near the contour boundaries.

intensities correlate well over the full width of the profile, but as seen in Fig. 2 the linear polarisation L and circular polarisation V shows a more complex behaviour. In L only the outer components correlate well, although the centre shows the strongest linear polarisation. In V, the wings appear uncorrelated because of their random signs but here the centre is strongly correlated. Anti-correlation regions (offset from the centre) indicate that RHC-LHC transition direction is maintained over the band. As the magnitude of circular polarisation |V| correlates well over the full profile we have evidence that uncorrelated flips between LHC & RHC are observable in the outer components of the profile but not in the centre. Our observations lead us to the conclusion that the emission process has a wide bandwidth ($> 2\nu_{\rm min}$) and that either the assumption of a lower origin of outer components (Rankin, 1990) is wrong or the observable fluctuations cannot be a propagation effect!

5 Unexpected Properties of Pulsars at High Radio Frequencies

The large and precisely formed collecting area of the 100 m telescope has been used for high frequency ($\nu > 10$ GHz) pulsar observations since the beginning in the early seventies (Wielebinski et al., 1972). We extended the frequency range for a number of pulsars up to 43 GHz and even detected PSR B0355+54 at 90 GHz on Pico Veleta (Morris et al., 1997). Using the Effelsberg telescope, equipped with a primary focus receiver at $\nu = 34$ GHz with a bandwidth of 2 GHz and a system temperature of $T_{\rm sys} = 100$ K we detected 8 pulsars (Wielebinski et. al. 1997). Even at $\nu = 43$ GHz (secondary focus, BW= 2 GHz, $T_{\rm sys} = 250$ K) we succeeded in detecting four of the sources (Kramer et at., 1997). An unexpected flattening or turn-over of their Spectra (Fig.3, left), or their particular strength (i.e. PSR B0355+54 with 0.5 mJy at 87 GHz) made the Pulsars visible at high radio frequencies (Kramer et al., 1996). This flattening of the spectrum has also been detected at

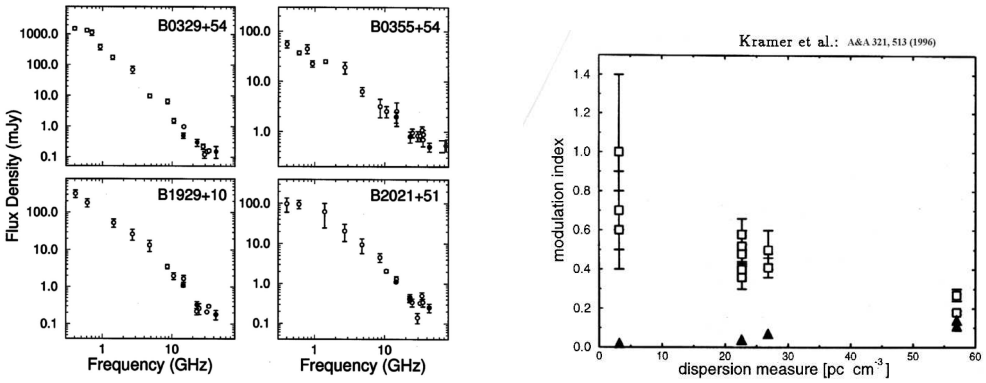

Fig. 3 *left:* Spectra of four pulsars observed up to 43 GHz, PSR 0355+54 has at least 0.5 mJy at 87 GHz, *right:* modulation index for five pulsars at 33 GHz, black triangles: predictions assuming weak interstellar scintillation.

a lower frequency limit (> 23 GHz) for a further pulsar: PSR B0144+59. In all cases we observed simple, Gaussian profile shapes,- the profile development saturates above 10 GHz, a high and increasing depolarisation, but the position angle is the same as at low ν. From the profile widths we estimated the high frequency emission heights to be around 100 km, - except for B1929+10 with 600 km. There was no indication of a deviation from dipolar geometry (Xilouris et al., 1996). Another surprising property of the high frequency radio emission from pulsars is its strong variability (Kramer et al., 1997). Fig. 3 (right) shows the observed modulation index m for five pulsars at 33 GHz and the theoretical predicitions from the $m \propto (\nu/\nu_{crit})^{-1.42}$ law pertaining to the weak insterstellar scattering regime. The critical frequencies were below 7 GHz in all the discussed cases. Such a variability cannot be explained by ordinary propagation effects in the ISM,- hence it is an intrinsic property of the propagation or the emission within the PSR magnetosphere. Furthermore,- we do not expect the spectrum to become flatter because of the propagation in the magnetosphere,- so there could be an indication of another emission mechanism appearing above 20-30 GHz and then taking over into the optical band.

6 Observational Limits on Plasma Densities and Energies

Electric charges in the inner parts of the PSR magnetosphere move only along the field lines,- their plasma frequency determines the lower frequency limits of effective plasma waves and instabilities. Depending on the actual emission mechanism, the minimum observable frequency at a given distance r from the neutron star is given by

$$\nu = \frac{\gamma^{\alpha-1/2}}{2\pi}\sqrt{\frac{n_{GJ}(r)\xi q_e^2}{\epsilon_0 m_e}} \tag{3}$$

The index is given as $\alpha = 1$ for a curvature emission process and $\alpha = 2$ for emission by coherent inverse Compton scattering and $n_{GJ}(r)$ is the distance-dependent co-rotation charge density together with the particle multiplicity $\xi \sim 10^4$. Solving for density and Lorentz factor we get a universal constraint linking the emission distance r, the Sturrock factor ξ and the Lorentz factor γ:

$$\xi\gamma^{2\alpha-1} = \frac{2\pi^2 m_e \nu^2}{q_e \Omega B_0}\frac{r^3}{r_{ns}^3}$$

$$= 1.8 \cdot 10^{-3} \left(\frac{\nu}{100\,\mathrm{MHz}}\right)^2 \left(\frac{P}{\mathrm{s}}\right) \left(\frac{10^{12}\mathrm{G}}{B_0}\right) \left(\frac{r}{r_{ns}}\right)^3 \tag{4}$$

For a "standard pulsar" with $B_0 = 10^{12}\,\mathrm{G}, P = 0.5\,\mathrm{s}, r = 50 r_{ns}$ we obtain $\xi\gamma < 1786$. This already shows, that the usual assumptions of $\xi = 10^4$ and $\gamma = 100$ are not compatible with the escape of low frequency radioemission from the observed emission regions. The situation is even more dramatic in the well researched case of PSR 0531+21 (Crab) where the maximum of the radio emission is at $\nu = 160\,\mathrm{MHz}$, and the other parameters are $B_0 = 3.0 \cdot 10^{12}\,\mathrm{G}, P = 0.033\,\mathrm{s}$. It is reasonable to assume, that the radio emission originates *within* the light cylinder ($r < 157 r_{ns}$), but in that case the 160 MHz radiation can only be produced (Kunzl et al., 1998) in a region where $\xi\gamma < 163$ which effectively rules out any high particle density inner gap pair production model for the crab pulsar.

7 Shortcomings of the Curvature Radiation Model

Curvature radiation can be described in terms of emission by a relativistic particle moving around the arc of a circle chosen such that the actual acceleration corresponds to centripetal acceleration. The critical frequency where most of the radiation is emitted depends only on the Lorentz factor γ of the the particles and the local radius of curvature R_c of the field line which is a simple function of distance from the star. It is approximately given by (e.g. Zheleznyakov 1996, p. 231)

$$\nu_c \simeq \frac{3c}{4\pi R_c}\gamma^3\,, \tag{5a}$$

Or if we observe a particular frequency we find the corresponding Lorentz factor via

$$\gamma \simeq \left[\frac{\nu_c 4\pi R_c}{3c}\right]^{1/3}. \tag{5b}$$

Together with the expression for the plasma frequency (3) we have two equations for the emitted frequency $\nu(\gamma, r)$ which enable us to determine the minimum emission height from $\nu \geq \omega_{\mathrm{pe}}/2\pi$ by using eq.(5b) to eliminate γ

$$\nu = \frac{3^{2/5}}{4\pi c^{1/5}}\left(\frac{8 q_e \Omega B_0 r_{ns}^3}{3 m_e}\right)^{3/5} r^{-9/5} R_c^{1/5}\,. \tag{6}$$

Coherent emission is required to explain the observed brightness temperatures and coherence exists in volumes of the order of $V_c = c^3\gamma^2/\pi\nu^3$ (Melrose 1991). The power output of such a coherence volume is then given by $P_N = \frac{2}{3}\gamma^4 (N_c \cdot q_e)^2 c/4\pi\epsilon_0 R_c^2$ with $N_c = V_c \cdot n_{\mathrm{GJ}}$ being the number of particles within a coherence volume. To account for the observed luminosity L one requires $N_v = \frac{L}{P_N} = 7 \cdot 10^{11}$ of these volumes, which implies a minimal size of the emission region $\Lambda_c = (N_v \cdot V_c)^{1/3}$ which is about 16 km for a typical pulsar. The energy loss of any single charge within the emission region is now $P_\Lambda = \frac{\Lambda_c}{c}\frac{P_N}{N_c}$, which must never exeed the energy of the particle $\gamma m_e c^2$ itself. We can express the efficiency, the ratio of emitted energy and total kinetic energy as

$$\eta_1 = \frac{P_\Lambda}{\gamma m_e c^2} \tag{7}$$

and evalute it along any field line where it cannot exceed unity because of *energy conservation*. Fig. 4 shows the results for five frequencies in the case of the well known Pulsar

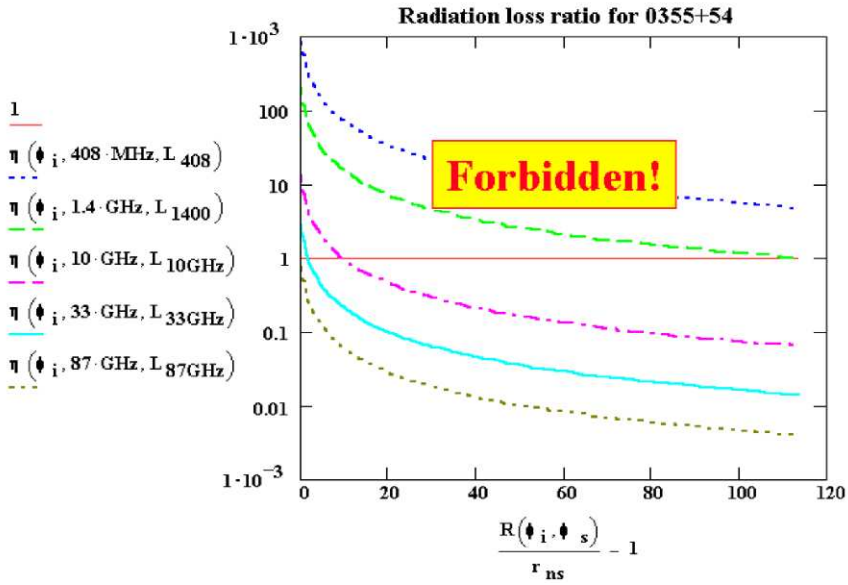

Fig. 4 PSR 0355+54: Required efficiency for conversion of kinetic beam energy into curvature radiation at five different frequencies. The upper half of the panel corresponds to a regime where the observed luminosity exceeds the energy budget of the streaming particles.

B0355+54 from which radio emission has been observed up to 87 GHz. Particles have only sufficient energies to provide the observed radio luminosities for frequencies above 10 GHz. Increases in density or particle energy would aggravate the problem. An increase in density corresponds to an increase in frequency $\propto n^{\frac{1}{3}}$ at a given radius and similarly an increase in the Lorentz factor of the particles increases the frequency again $\propto \gamma^3$. Hence coherent curvature radiation cannot be the mechanism for the low frequency radio emission, where most of the radio power is emitted.

ACKNOWLEDGEMENTS A. Karastergiou, M. Kramer, O. Löhmer, D. Mitra and R. Wielebinski provided material and I am grateful for their many helpful discussions and their support for this article.

References

Abrahams A.M., Shapiro S.L., ApJ, 1991, 374, 6552-667
Bartel N., Sieber W., A&A, 1978, 70, 260
Beck R., Space Sci. Rev., 2001, 99, 243
Child C.D., Phys. Rev., 1911, 32
Deutsch A., Ann. Astrophys., 1955, 18, 1, 1-10
Doroshenko O.V., Kopeikin S.M., MNRAS, 1995, 271, 1029
Doroshenko O.V., Löhmer O., Kramer M., et al., A&A, 2001, 379, 579
Georgelin Y.M., Georgelin Y.P., A&A, 1976, 49, 57
Karastergiou A., von Hoensbroech A., Kramer M., et al., A&A, 2001, 379, 270
Kramer M., Xilouris K.M., Jessner A., et al., A&A, 1996, 306, 867
Kramer M., Doroshenko O.V., Jessner A., et al., ApJ 1997, 488, 364
Kramer M., Xilouris K.M., Rickett B., A&A, 1997, 321, 513
Kunzl T., Lesch H., Jessner A., et al., ApJ, 1998, 505, L139
Lesch H., Jessner A., Kramer M., et al., A&A, 1998, 332, L21
Lyne A.G., Smith F.G., MNRAS, 1989, 237, 533
Löhmer O., Kramer M., Mitra D., et al., ApJ, 2001, 562, L157

Lorimer O., Jessner A., Seiradakis J.H., A&AS, 1998, 128, 541-544
Mitra D., Wielebinski R., Kramer M., et al., A&A, 2002, submitted
Morris D., Kramer M., Thum C., et al., A&A, 1997, 322, L17
Rand R.J., Lyne A.G., MNRAS, 1994, 268, 497
Stappers B.W., Bessel M.S., Bailes M., et al., ApJ, 1996, 465, L119
Taylor J.H., Cordes J.M., ApJ, 1993, 411, 674
Wielebinski R., Sieber W., Graham D.A., et al., Nature, 1972, 240, 131
Wielebinski R., Jessner A., Kramer M., et al., A&A, 1993, 272, L13-16
Xilouris K.M., Kramer M., Jessner A., et al., A&A, 1996, 309, 481